Surface recombination and out-of-plane diffusivity of free excitons in hexagonal boron nitride

Sébastien Roux [1,2] Christophe Arnold,[2] Etienne Carré,[1,2] Eli Janzen,[3] James H. Edgar,[3] Camille Maestre [4]
Bérangère Toury [4] Catherine Journet [4] Vincent Garnier [5] Philippe Steyer,[5] Takashi Taniguchi [6]
Kenji Watanabe [7] Annick Loiseau,[1,*] and Julien Barjon[2,†]
[1]*Laboratoire d'Etude des Microstructures, ONERA-CNRS, Université Paris-Saclay, BP 72, 92322 Châtillon Cedex, France*
[2]*Université Paris-Saclay, UVSQ, CNRS, GEMaC, 78000, Versailles, France*
[3]*Tim Taylor Department of Chemical Engineering, Kansas State University Manhattan, Manhattan, Kansas 66506, USA*
[4]*Laboratoire des Multimatériaux et Interfaces, UMR CNRS 5615, Université Lyon, Université Claude Bernard Lyon 1, F-69622 Villeurbanne, France*
[5]*Laboratoire MATEIS, UMR CNRS 5510, Université Lyon, INSA Lyon, F-69621 Villeurbanne, France*
[6]*Research Center for Materials Nanoarchitectonics, National Institute for Materials Science, 1-1 Namiki, Tsukuba 305-0044, Japan*
[7]*Research Center for Electronic and Optical Materials, National Institute for Materials Science, 1-1 Namiki, Tsukuba 305-0044, Japan*

(Received 11 August 2023; revised 23 March 2024; accepted 26 March 2024; published 22 April 2024)

We present an experimental protocol using cathodoluminescence measurements as a function of the electron incident energy to study both exciton diffusion in a directional way and surface exciton recombination. Our approach overcomes the challenges of anisotropic diffusion and the limited applicability of existing methods to the bulk counterparts of two-dimensional (2D) materials. The protocol is then applied at room and at cryogenic temperatures to four bulk hexagonal boron nitride crystals grown by different synthesis routes. The exciton diffusivity depends on the sample quality but not on the temperature, indicating it is limited by defect scattering even in the best quality crystals. The lower limit for the diffusivity by phonon scattering is 0.2 $cm^2\,s^{-1}$. Diffusion lengths were as much as 570 nm. Finally, the surface recombination velocity exceeds 10^5 $cm^2\,s^{-1}$, at a level similar to silicon or diamond. This result reveals that surface recombination could strongly limit light-emitting devices based on 2D materials.

DOI: 10.1103/PhysRevB.109.155305

I. INTRODUCTION

In most two-dimensional (2D) semiconductors, a surprising increase in the luminescence efficiency appears when reducing thickness at the atomic level, especially between bilayer and monolayer crystals where the band gap undergoes its indirect-to-direct transition [1–3]. However, in the specific case of hexagonal boron nitride (hBN), the bulk crystal exhibits a high radiative efficiency of up to 50% in cathodoluminescence (CL) [4], with a short radiative lifetime of 30 ns [5], which arises from the high compactness of its indirect excitons. Conversely, the luminescence intensity for hBN thin films [6] is dramatically decreased: there is no CL signal for less than six layers. The luminescence of the monolayer hBN free exciton has only recently been observed, thanks to extremely long photoluminescence experiments [7,8]. Moreover, a drastic change is observed between the free-exciton decay times of bulk samples measured down to a few tens of picoseconds in time-resolved photoluminescence [9–12] and those measured at several nanoseconds in our previous work with a bulk excitation in time-resolved CL [5]. The underlying reasons for the decrease in intensity with the thickness of the hBN layers, as well as the decrease in exciton lifetime with the depth of excitation, are not yet fully understood and elucidated. This will be investigated in this work in terms of surface effects and exciton diffusion.

Often ignored in 2D materials, surfaces play a well-known role in three-dimensional (3D) semiconductors in limiting light emission efficiency in standard optoelectronic devices. The rate of surface recombination of free charge carriers is governed by the physical properties of the defect states at the surface, so that it could be reduced by using passivation strategies [13–15]. It is quantitatively characterized by a parameter called the surface recombination velocity, s, which typically ranges between 1 and 10^6 cm s^{-1}, depending on the material and its surface termination [13,15–17]. In hBN, due to the sp^2 orbital hybridization, all chemical bonds are satisfied between atoms on the same atomic plane, so there are no dangling bonds at the surface. Considering this, the surface recombination rate for free carriers should be low in hBN compared to sp^3 hybridized semiconductors with dangling bonds [13]. However, strong surface effects are suggested by the low luminescence efficiency of hBN crystals of a few atomic layers [6]. In hBN, and more generally in 2D materials, surface recombinations are still unexplored and remain an open question.

Surface recombination and the associated luminescence losses are promoted by the diffusion of charge carriers injected into the volume of a crystal towards its surfaces. In the context of lamellar materials, such as the 2Ds, the out-of-plane

*annick.loiseau@onera.fr
†julien.barjon@uvsq.fr

 ©2024 American Physical Society

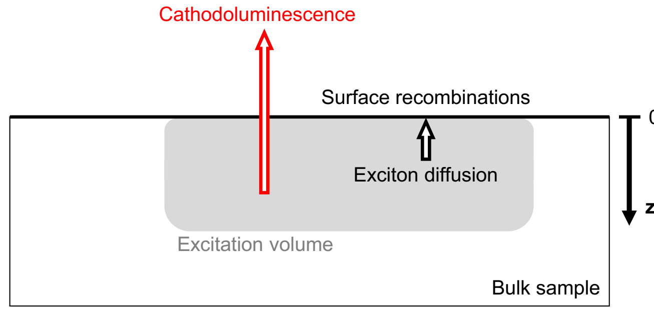

FIG. 1. Scheme of the CL experiment in a 1D geometry to analyze the out-of-plane exciton diffusion in the bulk crystal and the recombination properties of the surface.

diffusivity is the key parameter for understanding the surface recombination properties. Furthermore, understanding exciton diffusion in 2D semiconductors is of strategic importance for the development of new "excitronic" devices based on the control of exciton flux, which has attracted attention with the advent of 2D heterostructures [18–21]. However, experiments and devices have only focused on the in-plane exciton diffusion in 2D monolayers of transition-metal dichalcogenides [22–24].

The study of exciton diffusion can be carried out by PL experiments using various pump-probe techniques [25,26], or by CL experiments, which benefit from a better control of the excitation volume, down to tens of nm^3, by analyzing the transfer of excitons from a localized excitation to a physical probe [27–32]. To properly analyze such experiments, one must decouple the combined effects of (i) in-plane diffusion, (ii) out-of-plane diffusion, (iii) surface recombinations, and (iv) inhomogeneous in-depth energy deposition. Due to the anisotropy and the still-unexplored surface recombination properties of 2D materials, the use of traditional protocols for their out-of-plane exciton diffusion poses significant challenges.

This work presents an experimental protocol in CL that provides a powerful tool for investigating the out-of-plane diffusion and the surface recombination properties of a bulk crystal using a one-dimensional (1D) excitation geometry. The method is applicable to all types of semiconductors, including those with anisotropic diffusion, and does not require prior knowledge of the surface recombination properties. After introducing the principle of the experiment, a theoretical analysis of diffusion is given, providing an analytical description of experimental results. The method is then applied to four bulk hBN samples at room and cryogenic temperature, allowing the evaluation of out-of-plane diffusion length, diffusion constant, surface recombination velocity, and their dependence on the crystal quality and temperature.

II. ANALYTICAL MODEL FOR A 1D DIFFUSION EXPERIMENT IN CL

We first present the principle of the CL experiment. As illustrated in Fig. 1, a 1D diffusion geometry is obtained by significantly defocusing the incident electron beam, which allows lateral diffusion and side effects to be neglected. The CL intensity is measured as a function of the excitation depth, which is modulated by varying the acceleration voltage of the incident electrons. At low excitation depths, surface recombination effects lead to a reduction of the CL intensity, and the key point is to use the recombinant surface as a probe for exciton diffusion. The quantitative analysis of such an experiment requires consideration of two essential aspects: (i) the development of a simple and quantitative description of the excitation depth as a function of the acceleration voltage, and (ii) the establishment of an analytical model that explains the decrease in CL intensity at low excitation depths, taking into account the surface effect in relation to the relevant physical parameters. We first address these two issues theoretically.

The free-exciton[1] concentration $n(z)$ that is established under steady-state generation rate $\mathcal{G}$ in a semiconductor crystal results from the diffusion equation studied here in a 1D symmetry:

$$D\frac{\partial^2 n}{\partial z^2} - \frac{n}{\tau} + \mathcal{G} = 0, \tag{1}$$

where D is the exciton diffusivity along the z axis, and its determination is one of the goals of the CL experiments. τ is the exciton lifetime in the bulk of the crystal, i.e., far from the surface. It is measured by time-resolved CL experiments at high voltage, as detailed in a previous work [5].

We consider here a semi-infinite crystal surrounded by vacuum for $z < 0$. The surface recombinations at $z = 0$ are described as a boundary condition of the diffusion equation, with the surface recombination velocity s:

$$D\left[\frac{\partial n}{\partial z}\right]_{z=0} = s\, n(0). \tag{2}$$

Dealing with an arbitrary in-depth profile of the generation rate $\mathcal{G}$ due to an excitation spread in depth is not straightforward. Analytical solutions can be found when the excitation in depth follows an exponential decay (e.g., optical absorption). However, the excitation profile with electrons has no general description with analytical expressions. To treat this problem it is necessary to decompose a realistic excitation profile, e.g., that obtained by Monte Carlo simulation, with planar sources. The solution for a planar source located at the depth $z = z'$ is a Green's function that was formulated in 1955 by Van Roosbroeck [33], where the depth distribution of particles in the crystal is defined separately on each side of the generation plane. It could be written

$$f_{z',a}(z) = \begin{cases} \frac{1}{2L}e^{-\frac{z'}{L}}\left(e^{\frac{z}{L}} + ae^{-\frac{z}{L}}\right) & \text{if } z \leqslant z' \\ \frac{1}{2L}e^{-\frac{z}{L}}\left(e^{\frac{z'}{L}} + ae^{-\frac{z'}{L}}\right) & \text{if } z \geqslant z' \end{cases}, \tag{3}$$

where $L = \sqrt{D\tau}$ is the diffusion length along the z axis. An interpretation of this result with virtual image sources is as follows: the recombinant surface at $z = 0$ might be viewed as a semireflecting mirror for the real sources in the crystal, with a reflection coefficient $a = \frac{1-S}{1+S}$. In this expression, $S = \frac{s}{v_D}$ is the reduced recombination velocity, i.e., normalized by the diffusion velocity $v_D = \frac{L}{\tau} = \sqrt{\frac{D}{\tau}}$. The limiting cases are

[1] Assuming strongly bound excitons, i.e., negligible free-carrier concentrations.

$S = +\infty$ ($a = -1$) for a surface with infinite recombination velocity and $S = 0$ ($a = 1$) associated with total reflection.

Since the diffusion equation is linear, an arbitrary in-depth profile of exciton generation $g(z)$ normalized such that $\int_0^{+\infty} g(z)dz = 1$ results in an exciton concentration distribution that is written here[2]:

$$n(z) = \frac{G\tau}{\mathcal{A}} \int_0^{+\infty} f_{z',a}(z)g(z')dz'. \tag{4}$$

This expression indicates how excitons are distributed in the semiconductor crystal by the combined effects of diffusion from a given excitation profile and recombinations at the crystal surface. The prefactor contains the experimental parameters of a CL experiment. $\mathcal{A}$ is the area of the electron beam impinging on a 3D crystal. Experimentally one should ensure that $\mathcal{A} \gg L^2$ to assume a 1D diffusion. For instance, the electron-beam spot should be sufficiently defocused to be much larger than the in-plane diffusion length (see Fig. 1). G (s^{-1}) is the electron-hole generation rate in the semiconductor. $G = \frac{(1-\alpha)Vi}{\langle E_{eh}\rangle}$ is a simple function of the acceleration voltage V, the beam current i, the backscattering factor α, and the average electron-hole energy $\langle E_{eh}\rangle$ required for the formation of an electron-hole pair. $\langle E_{eh}\rangle \approx 3E_g$ is a commonly used relation as a function of the band-gap energy E_g when $\langle E_{eh}\rangle$ is not known experimentally for the material of interest [34].

The recombinations at the crystal surface at $z = 0$ are responsible for exciton losses and *in fine* for a decrease of their luminescence intensity I. Instead of integrating Eq. (4) over the crystal volume to evaluate the total number of steady-state excitons in the crystal, the quantity of lost excitons N' is calculated more directly [35] considering the diffusion flux at $z = 0$:

$$N' = D\left[\frac{\partial n}{\partial z}\right]_{z=0} \mathcal{A}\tau, \tag{5}$$

which gives the following result after calculation:

$$\frac{N'}{N} = \frac{(1-a)}{2} \int_0^{+\infty} e^{-\frac{z'}{L}} g(z')dz', \tag{6}$$

where $N = G\tau$ is the steady-state exciton population in a crystal without surface losses ($s = 0$). The luminescence intensity I is proportional to the total number of excitons present in the crystal under steady-state excitation, via the constant radiative rate of excitons. Noting I_0 the luminescence intensity when surface recombination is negligible, measured experimentally in the high-voltage limit, we obtain $\frac{I}{I_0} = 1 - \frac{N'}{N}$. Finally, the steady-state CL intensity is

$$\frac{I}{I_0} = 1 - \frac{(1-a)}{2} \int_0^{+\infty} e^{-\frac{z'}{L}} g(z')dz'. \tag{7}$$

Various analytical functions have been proposed to describe $g(z)$, the in-depth profile of excitation by an electron beam as a function of its acceleration voltage [36,37]. Their success was limited for quantitative analysis of cathodoluminescence experiments because their validity is restricted to limited ranges of acceleration voltage and material density.

[2] $g(z) = \delta(z - z')$ for a plane source at $z = z'$.

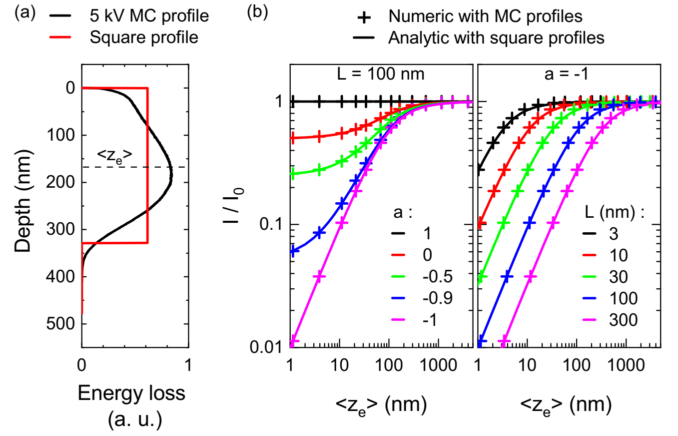

FIG. 2. (a) Generation profile for a 5-kV incident electron beam in hBN calculated by MC simulations (in black) and its square approximation (in red). Both profiles share the same mean excitation depth $\langle z_e\rangle$ calculated by MC simulation. (b) I/I_0 as a function of $\langle z_e\rangle$ for a steady excitation inside the crystal. The results are obtained either numerically with discrete generation profiles from MC simulations (cross) or analytically with Eq. (8) considering the square profile.

Today, Monte Carlo (MC) algorithms are preferred, since they provide simulations of electron energy losses in a simple and relatively accurate way [38]. As shown in Appendix A, the in-depth distribution of the generation rate can be assessed numerically with Monte Carlo simulations as well as the acceleration voltage dependence of the mean excitation depth $\langle z_e\rangle = \int_0^{+\infty} zg(z)dz$. An example of a calculated profile for a 5-kV acceleration voltage is shown in Fig. 2(a) together with the corresponding value of $\langle z_e\rangle$.

Considering its shape, this profile can be approximated by a square profile also shown in Fig. 2(a) and defined by a depth distribution $g(z) = \sqcap(z)$, with a constant generation rate down to an electron stopping depth $R = 2\langle z_e\rangle$, i.e.,

$$\sqcap(z) = \begin{cases} 1/R & \text{if } 0 \leqslant z \leqslant R \\ 0 & \text{if } z > R \end{cases}.$$

Using this simpler depth distribution is of key interest since its provides an analytical expression of $\frac{I}{I_0}$ involving three parameters, namely, a, L, and $\langle z_e\rangle$:

$$\frac{I}{I_0} = 1 - \frac{(1-a)}{2} \frac{1 - e^{-\frac{2\langle z_e\rangle}{L}}}{\frac{2\langle z_e\rangle}{L}}. \tag{8}$$

Figure 2(b) depicts the variations of $\frac{I}{I_0}$ as a function of $\langle z_e\rangle$ for different values of a and L as generated from the analytical equation Eq. (8). They are compared with numerical calculations of $\frac{I}{I_0}$ obtained by discretizing the integral term in Eq. (7) to inject the generation profiles $g(z)$ obtained from MC simulations.

This comparison attests that an excellent agreement is found between analytical and numerical methods. This remarkable result shows that the precise shape of the generation profile $g(z)$ has a negligible effect on the luminescence intensity, while the mean excitation depth $\langle z_e\rangle$ turns out to be the critical parameter for the interpretation of these CL experiments. This observation holds true even for GaN, which

has a significantly higher density (6.15 g cm^{-3}) than hBN (2.18 g cm^{-3}), resulting in drastically different excitation profiles (see Appendix B). Thus, it turns out that the analytical description of Eq. (8) can be applied to a wide range of semiconductor materials, provided that the CL reabsorption by the crystal remains negligible, which is the case in indirect-band-gap semiconductors, for instance[3] [39].

Figure 2(b) also reveals that the parameters a and L have distinct influences on the $\frac{I}{I_0}(\langle z_e \rangle)$ curve. In particular, the parameter a determines the shape of the curve at low excitation depths, while the parameter L governs the position of the curve along the horizontal axis. This observation provides the guidance for the analysis of experimental measurements. Provided that the acceleration voltage is varied over a sufficiently large range, the analytical description of Eq. (8) has the ability to accurately fit experimental measurements of the CL intensity with reliable values of the diffusion length L and the parameter a which quantifies the level of surface recombinations. Further, combining these experiments with measurements of the bulk exciton lifetime τ using time-resolved CL at high voltage gives access to the evaluation of the diffusivity D and the surface recombination velocity s, which are the key physical quantities of interest.

III. EXPERIMENTAL RESULTS FOR FREE EXCITONS IN HBN: ANALYSIS AND DISCUSSION

We now turn to the experiments. Four bulk hBN crystals were investigated. One was grown at Kansas State University using an atmospheric pressure high-temperature process [40–42] from Ni/Cr solvent and natural boron isotopic content (APHT sample). Two crystals were synthesized at the NIMS Laboratory using a high pressure high temperature route [43,44] (samples HPHT1 and HPHT2). And the last crystal was grown in the LMI Laboratory using a polymer-derived ceramic method [45,46] (PDC sample). The HPHT samples are widely recognized in the 2D material scientific community as reference hBN materials. Prior to analysis, the samples were cleaved to obtain a clean, uncontaminated surface and then mounted on conducting doped silicon wafers. A conductive bond was established on one edge of the crystal using Ag paint. This mounting allows an efficient charge evacuation during electron-beam irradiation. The thickness of the crystals was measured to be greater than 10 μm using a mechanical profilometer, while the lateral size exceed hundreds of micrometers.

Cathodoluminescence spectra were collected using a scanning electron microscope (SEM) JEOL7001F equipped with a Horiba Jobin-Yvon CL system optimized for UV spectroscopy, as described in detail in Ref. [4]. To avoid nonlinear effects such as exciton-exciton annihilation [47], a low excitation power of about 1 μW was employed. To achieve a 1D geometry configuration (shown in Fig. 1), the electron beam was significantly defocused, resulting in an excitation spot size of 3.5 μm. The signal from the whole excited area is collected thanks to a parabolic mirror and transmitted to the detectors. The excitation depth was controlled by varying the electron acceleration voltage from 500 V to 20 kV. For each acceleration voltage, the CL intensity I measurements were normalized by the excitation power $P = iV \cdot (1 - f)$, taking into account slight variations (±10%) in the incident electron-beam power (iV) at each acceleration voltage V, as well as the voltage dependence of the electron backscattering factor α (see Appendix A). The uncertainty in the CL intensity was estimated to be 20%. Finally, time-resolved CL was performed using a custom-built beam blanker installed in the SEM column, achieving a temporal resolution of 100 ps (details of the setup can be found in [5]). The time-resolved CL signal was filtered at 215 +/− 7.5 nm to select only the free-exciton emission in the analysis. Figure 3 presents an application of the protocol to the APHT sample. In Fig. 3(a) the CL intensity I/I_0 is plotted as a function of the mean excitation depth $\langle z_e \rangle$ as extracted from Monte Carlo simulations. At high excitation depths, the intensity plateau indicates that excitons are generated too far from the top surface to cause significant surface effects. The decrease in luminescence intensity at low excitation depths is attributed to surface recombinations enhanced by exciton diffusion towards the top surface. Fit of the experimental data by Eq. (8) is discussed from Fig. 3(a). Taking into account the uncertainties, the 95% confidence interval for L is between 84 and 100 nm, and the best fit is with $L = 92$ nm and $a = -1$, as shown in Fig. 3(a). This figure also illustrates that only a few points at low excitation depths contribute to the determination of the parameter a. Equation (8) is displayed for $L = 92$ nm and $a = -1$, $a = -0.9$, and $a = -0.8$. To avoid being influenced by a potential outlier, we choose a lower bound for a such

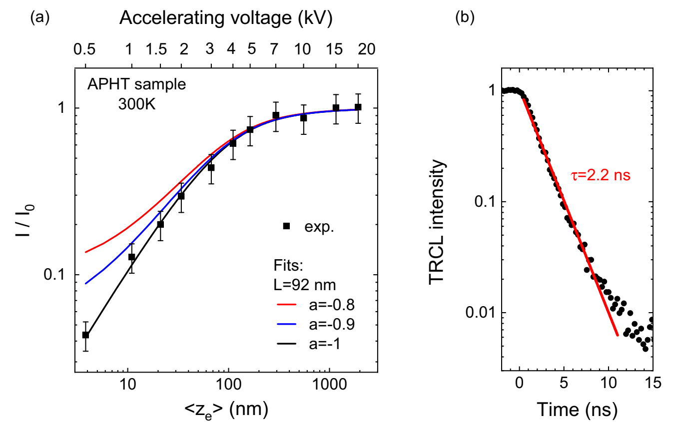

FIG. 3. (a) CL intensity I/I_0 as a function of the acceleration voltage and the corresponding mean excitation depth $\langle z_e \rangle$ (see Appendix A). The analytical equation, Eq. (8), is depicted for a diffusion length L of 92 nm and various values of the parameter a. (b) Temporal decay of the free-exciton luminescence filtered at 215 ± 7.5 nm measured in the same area after the interruption of a 15-kV electron beam. The bulk lifetime of the free exciton τ is determined by fitting the data with an asymptote.

[3]The present model is inspired by the early works of Wittry *et al.* in 1967 [39]. Despite the title of their paper, "Measurement of Diffusion Lengths in Direct Gap Semiconductors by Electron Beam Excitation," the present work rather applies to indirect semiconductors, since the efficient luminescence reabsorption in direct-band-gap semiconductors requires careful consideration when evaluating luminescence intensity.

TABLE I. Results of the CL experiments on the four bulk hBN samples at 300 K: the out-of-plane exciton diffusion length L, the parameter a, and the exciton lifetime τ. The diffusivity $D = L^2/\tau$ and an estimate of a lower bound of the surface recombination velocity $s = \frac{L}{\tau}\frac{1-a}{1+a}$ are derived.

	L (nm)	a	τ (ns)	s (cm/s)	D (cm^2/s)
HPHT1	570	< -0.98	16.5	$>3 \times 10^5$	0.20 ± 0.07
HPHT2	246	< -0.96	8.4	$>1 \times 10^5$	0.07 ± 0.03
APHT	92	< -0.9	2.2	$>7 \times 10^4$	0.04 ± 0.01
PDC	< 5	–	0.03	-	<0.02

that the corresponding fit misses at least two points of the experimental dataset. From Fig. 3(a) we extract $a < -0.9$ on the APHT sample. Note that this seems to be a safe estimate since the fitted curve with $a = -0.9$ is already quite far from the experimental point measured at 0.5 kV. These results make it possible to evaluate and discuss the diffusivity D and the surface recombination velocity s by starting with the latter. The surface recombination velocity $s = \frac{L}{\tau}\frac{1-a}{1+a}$ is known from L, τ, and a. The exciton lifetime τ is measured independently by time-resolved CL with an uncertainty of 10%, following the procedure described in [5] and shown in Fig. 3(b). Knowing the upper limit of a, a lower limit for the surface recombination velocity s is deduced, yielding $s > 7 \times 10^4$ cm/s for the APHT sample.

The high value of s is very robust as it could be confirmed from the analysis of data obtained from the different samples and at various temperatures (as shown in Tables I and II). The data sets are systematically best fitted with an adjustment value of $a = -1$, and the higher bounds of a extracted with the same precautions as on the APHT sample lead to a refinement of the lower limit of s to 10^5 cm/s at 6 and 300 K.

This is definitely a surprisingly high value, approaching the highest levels reported around 10^6 cm/s for 3D semiconductors such as in GaAs [16] and diamond [17]. A possible explanation for this result could be the presence of defects at the hBN surface. While it is challenging to completely rule out this possibility, note that the surfaces studied in this work were clean and freshly cleaved, minimizing potential contamination. In addition, there is no change in the shape of the spectra with the depth of excitation, as shown by the spectra in Appendix C, suggesting a defect concentration homogeneous in depth and a surface free of contamination. Another possible explanation relates to the surface exciton states that have been identified theoretically [48] and experimentally [4] in hBN and which are approximately 100 meV below the bulk hBN exciton. These surface states suggest that the hBN surface acts as a sink for excitons, with a sufficient energy depth to capture

TABLE II. Results of the CL experiments at 6 and 300 K on the HPHT1 sample.

T° (K)	L (nm)	a	τ (ns)	s (cm/s)	D (cm^2/s)
300 K	570	< -0.98	16.5	$>3 \times 10^5$	0.20 ± 0.07
6 K	275	< -0.95	3.0	$>3 \times 10^5$	0.25 ± 0.08

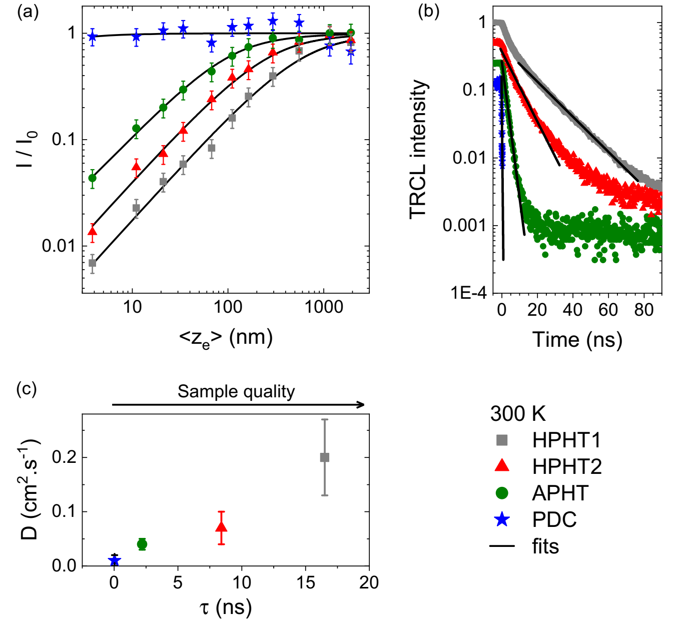

FIG. 4. (a) I/I_0 as function of the mean excitation depth $\langle z_e \rangle$, and (b) temporal decays of the free-exciton luminescence after interruption of a 15-kV steady excitation at $t = 0$, recorded on HPHT1, HPHT2, APHT, and PDC samples. The out-of-plane diffusion length L is deduced by fitting Eq. (8) in (a), while the bulk exciton lifetime τ is measured by time-resolved CL in (b). (c) Diffusivity as function of the exciton lifetime τ for the four samples. Note that τ is used to quantitatively compare the global quality of the samples.

them efficiently at room temperature, consistently with the high surface recombination rate observed in hBN.

Whatever its origin, the importance of surface recombination in hBN allows us to understand the difficulty of measuring the luminescence of its atomic layers. In the presence of such a high surface recombination rate, the luminescence of hBN crystals made of a few atomic layers is inevitably very low, as experimentally measured by Schué *et al.* [6]. Contrary to initial assumptions, the surfaces of 2D materials can also limit the efficiency of their luminescence, emphasizing the need to passivate them for use in optoelectronic devices. Recent studies on atomic layers of transition-metal dichalcogenides (TMDs) have demonstrated that the luminescence quantum yields only reach unity when the material is properly passivated [49,50]. The increase in quantum efficiency following passivation indicates that nonradiative recombinations occur at the TMD-air surface. Similar passivation techniques should be considered to mitigate nonradiative recombinations at the hBN surface, thereby enabling enhanced luminescence intensity and improving the potential of hBN for optoelectronic applications.

We now focus on the diffusion properties. The measured diffusion lengths L and the exciton lifetimes τ on the four samples at 300 K are depicted in Figs. 4(a) and 4(b). In the case of the PDC sample, the exciton lifetime is too short to be measured directly by time-resolved CL. However, using the linearity relationship between τ and the CL efficiency given in Ref. [5], the exciton lifetime τ on this sample was estimated as 0.03 ± 0.015 ns from the measurement of a 0.1%

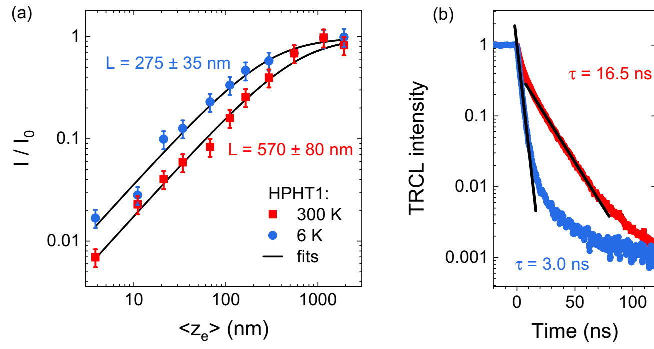

FIG. 5. (a) I/I_0 as function of the mean excitation depth $\langle z_e \rangle$ during continuous excitation and (b) temporal decays of the free-exciton luminescence after interruption of the 15-kV electron beam, recorded on the HPHT1 sample at 6 and 300 K. The best fit plots in (a) are obtained with $a = -1$ and the L values indicated on the graph.

CL efficiency (see details of the measurement in Ref. [4]). For all other samples, τ is measured directly by time-resolved CL with a 10% uncertainty. Considering the uncertainty of the CL intensity measurement, the 95% confidence intervals of L are always found within ± 15%. Finally, the diffusivity D is extracted considering the relation $D = L^2/\tau$ and taking into account the uncertainty in L and τ. The results are reported in Table I. As explained in Ref. [5], the higher the quality of the sample, the longer the exciton lifetime is. In Fig. 4(c) the exciton lifetime τ is used to quantitatively compare the global quality of the four samples. The figure exhibits a variation of the diffusivity D of more than one order of magnitude between the different samples and clearly demonstrates that the diffusivity is affected by the defects present in the samples. Figure 5 presents the measurements of the diffusion length L and exciton lifetime τ on the best sample (HPHT1) at both 6 and 300 K using our experimental protocol. The corresponding results are summarized in Table II. The diffusivity is 0.25 ± 0.08 cm^2/s at 6 K and 0.20 ± 0.07 cm^2/s at room temperature. The difference is not significant given the uncertainties of the measurement. In the case of intrinsic diffusion limited by phonon scattering, the diffusion constant at cryogenic temperatures is expected to be several orders of magnitude higher than at room temperature [51]. Our results indicate that even in the highest-quality HPHT1 sample, exciton diffusion is not limited by phonon scattering but rather by scattering on defects. This is consistent with impurity concentrations of oxygen and carbon on the order of 10^{18} cm^{-3} or below measured in the reference HPHT samples [44,52], a value which remains high compared to ultrapure semiconductors (10^{11}–10^{13} cm^{-3} typically) where the intrinsic diffusivity is reached [51].

We also note that in this sample an increase of the exciton lifetime is observed from 3 ns at 5 K to 16.5 ns at 300 K. The internal quantum efficiency (IQE) measured simultaneously at high voltage (with the method described in [4]) follows the same five-times increase: 13 ± 6% at 5 K and 60 ± 30% at 300 K. The radiative lifetime of the free exciton at 300 K (28 ns), which we can derive from both IQE and τ, is in good agreement with our previous investigations (27 ns) [5]. More interestingly, the radiative lifetime of free excitons is found to be almost constant in the investigated temperature range (23 ns at 5 K). Given the high energy of the phonons involved in the optical transition, this finding is consistent with the temperature dependence that is theoretically expected for radiative lifetime of indirect excitons [53]. The origin of nonradiative channels at low temperature would deserve to be investigated but is beyond the scope of this paper.

An estimate of the lower limit of the intrinsic diffusivity in hBN is provided by the highest value measured on our sample: $D > 0.2$ cm^2/s. Few values of the exciton diffusion constant are available in the literature for comparison, since excitons in standard semiconductors are weakly bound and generally dissociated at room temperature. Among them, the diffusion constant is 5 cm^2/s in diamond at 300 K [51]. In organic semiconductors where the diffusion is limited by exciton hopping from site to site, D is found in the range 10^{-6} to 0.01 $\text{cm}^2\,\text{s}^{-1}$ [54]. The lower bound found for D in hBN indicates that the hypothesis of a hopping diffusion mechanism can be safely discarded in this material, which has a diffusion constant typical of standard semiconductors.

IV. CONCLUSION

In conclusion, we have developed a CL protocol thanks to which the out-of-plane exciton diffusion length L, the diffusivity D, and the surface recombination velocity s have been recorded in a 2D semiconductor. It consists in recording the emitted light as a function of the acceleration voltage over a large range and using a widely defocused beam to be in 1D geometry. By a detailed analysis of the 1D diffusion equation applying to these CL experiments, we show that the emitted light in the presence of surface recombinations and diffusion is not affected by the in-depth profile of the exciton generation function but by the mean excitation depth $\langle z_e \rangle$ identified as the key parameter for our experiment. A simple analytical function is derived to describe the experimental results and to estimate the physical quantities in turn. The application of the protocol to four bulk hBN samples reveals diffusion lengths L of up to 570 nm at 300 K in the best crystal. From temperature-dependent experiments, the exciton diffusivity is shown to be limited by defect scattering. We conclude that the intrinsic diffusivity is superior to the highest value measured in this work, i.e., 0.2 cm^2/s, in good line with the order of magnitude for standard semiconductors. Finally, the surface recombination velocity of hBN is extremely high, at least at the level of silicon or diamond. This result explains the much shorter exciton lifetimes observed in the literature in photoluminescence where the excitation is superficial. Consequently, the exciton decay in time-resolved photoluminescence might be shortened by the surface effects. The efficient surface recombinations also explain the low luminescence intensity reported for hBN thin films and, more generally, indicates that exciton recombination at surfaces could be a strong limitation for light-emitting devices based on 2D materials.

ACKNOWLEDGMENTS

The research leading to these results has received funding from the European Union's Horizon 2020 Research and Innovation Program under Grant Agreements No. 785219

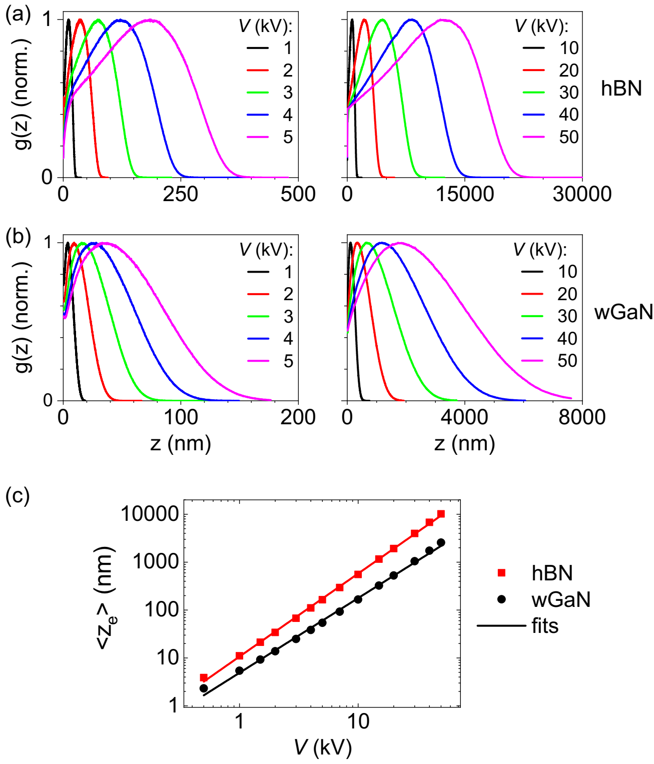

FIG. 6. Generation rate $g(z)$ as a function of depth z, in hBN (a) and wGaN (b). They were calculated by Monte Carlo simulations for different acceleration voltages V of the incident electron beam. (c) Mean excitation depth $\langle z_e \rangle$ as a function of acceleration voltage V extracted from the g(z) profiles shown in (a). The results are fitted by power laws

(Graphene Core 2) and No. 881603 (Graphene Core 3). Support for the APHT hBN crystal growth comes from the Office of Naval Research, Award No. N00014-20-1-2474. K.W. and T.T. acknowledge support from the JSPS KAKENHI (Grants No. 21H05233 and No. 23H02052) and World Premier International Research Center Initiative (WPI), MEXT, Japan.

APPENDIX A: MONTE CARLO SIMULATIONS TO EVALUATE THE IN-DEPTH ENERGY LOSSES OF INCIDENT ELECTRONS

Monte Carlo (MC) simulations using Casino V2.42 software [38] have been used to evaluate the in-depth distribution of electron energy losses in two different materials: hexagonal boron nitride (hBN, density 2.18 g cm^{-3}) and wurtzite gallium nitride (wGaN, density 6.15 g cm^{-3}). The simulations were performed to support the experimental study on hBN and to test the analytical model on a denser material (wGaN). The simulations followed the path of 10^6 incident electrons for each acceleration voltage (V) in the respective materials. The energy losses were calculated as a function of depth, and the mean excitation depth $\langle z_e \rangle = \int_0^{+\infty} z g(z) dz$ was determined (Fig. 6 and Table III). The results reveal that the in-depth profiles of energy losses present asymmetry and significant differences between hBN and wGaN, as shown in the figures. Note the different scales on the horizontal axes for hBN and wGaN, illustrating the lower penetration depth of the incident electrons in the denser wGaN material.

The excitation power applied to the sample can be determined using the relation $P = iV(1-\alpha)$, where i and V are the current and the acceleration voltage of the incident electron beam, and α corresponds to the loss due to backscattering of incident electrons. The parameter α can be calculated from the Monte Carlo simulations (results in Table III). The excitation power P is used to normalize the cathodoluminescence (CL) intensity (see main text).

Figure 6(c) presents the mean excitation depth $\langle z_e \rangle$ as a function of the acceleration voltage V within the range of 500–50 kV. The data follow power laws, namely, $\langle z_e \rangle_{\text{hBN}} = 10.67\ \text{V}^{1.73}$ and $\langle z_e \rangle_{w\text{GaN}} = 4.89\ V^{1.56}$, where $\langle z_e \rangle$ is given in nanometers and V is in kilovolts. It is worth noting that these power laws align well with the empirical relations used in the past, such as the Kanaya-Okayama equation [36], which describes the stopping depth of electrons with a power dependence of 5/3.

APPENDIX B: VALIDATION OF THE ANALYTICAL MODEL ON HBN AND GAN

Figure 7 depicts a theoretical calculation of I/I_0 as a function of $\langle z_e \rangle / L$, where $\langle z_e \rangle$ represents the mean excitation depth and L denotes the axial diffusion length. The calculation takes into account the realistic in-depth excitation profiles obtained from Monte Carlo simulations (refer to Fig. 6), as well as simplified square profiles [see Fig. 2(a)]. The comparison is made between two materials with different densities: hBN (2.18 g/cm^{-3}) and wGaN (6.15 g/cm^{-3}). The abscissa is dimensionless thanks to a normalization by L, in order to explore all the couples [L; a].

The figure demonstrates a remarkable agreement between the results obtained using Eq. (8), which solely considers the mean excitation depth $\langle z_e \rangle$, and the results obtained from Monte Carlo simulations incorporating the in-depth excitation profile through the discretized equation, Eq. (7). This agreement holds true for both light materials such as hBN

TABLE III. Mean excitation depth $\langle z_e \rangle$ and backscattering factor α, calculated from the Monte Carlo simulations on hBN and wGaN for different acceleration voltages V.

	V (kV)	0.5	1	1.5	2	3	4	5	7	10	15	20	30	40	50
hBN	$\langle z_e \rangle$(nm)	3.9	11	21	34	68	111	164	295	555	1160	1930	3980	6790	10200
	α	0.1	0.08	0.07	0.06	0.06	0.05	0.05	0.05	0.04	0.04	0.04	0.04	0.03	0.03
wGaN	$\langle z_e \rangle$(nm)	2.3	5.4	9.2	14	25	38	54	92	167	324	525	1050	1730	2570
	α	0.27	0.27	0.26	0.26	0.25	0.25	0.25	0.25	0.24	0.24	0.24	0.24	0.23	0.22

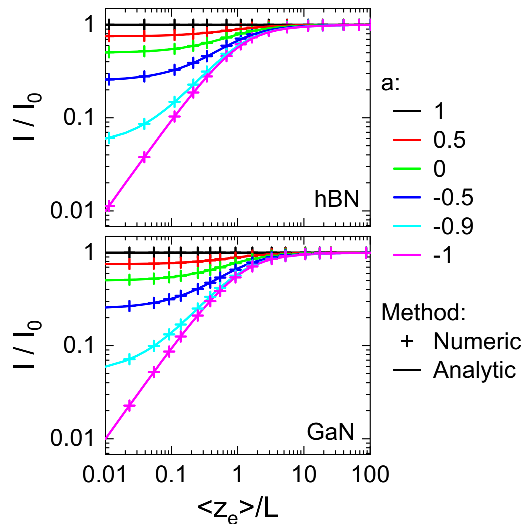

FIG. 7. I/I_0 as a function of $\langle z_e \rangle /L$. The results are obtained numerically using the generation profiles from the Monte Carlo simulations (cross) on hBN and GaN, and analytically with the square generation profile approximation [see Fig. 2(a)].

and heavier materials like wGaN, and regardless of the values of the parameters a and L. This validation demonstrates that $\langle z_e \rangle$ is the key parameter to interpret our experiment and that the analytical expression is applicable to fit the experimental results for a wide range of semiconductors and to deduce L and a.

APPENDIX C: SPECTRA RECORDED ON THE HPHT2 SAMPLE

Figure 8 shows the spectra obtained on the HPHT2 sample at 300 K and for different acceleration voltages ranging

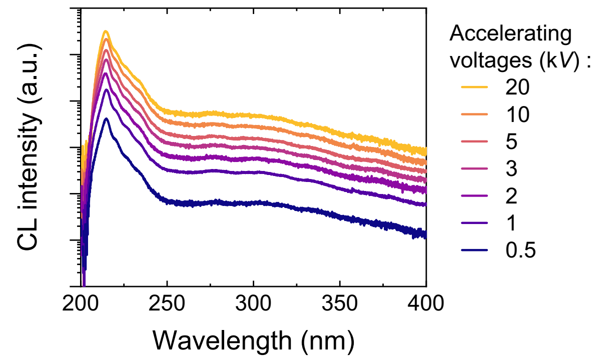

FIG. 8. Spectra acquired on HPHT2 sample at 300 K for different acceleration voltages and with a constant excitation power of 1 μW.

between 500 V and 20 kV. The spectra are corrected by the spectral response of the detector, following the procedure described in Ref. [4]. They are dominated by the free-exciton luminescence which appears at 300 K as a broad band between 200 and 240 nm with a maximum at 215 nm [4]. Defect-related luminescence appears at higher wavelengths [55], here with a low intensity. The intensity I/I_0, which is used in the main text, is extracted from the integrated area of the spectra between 200 and 240 nm.

As observed in Fig. 8, the shape of the spectra is identical regardless of the acceleration voltage, which means that it does not depend on the depth of excitation. This suggests that the crystal is extremely homogeneous in depth and presents a surface free of contamination. The decrease in intensity observed at low acceleration voltage is then attributed to the recombination of excitons at the top surface of the hBN crystal rather than to the presence of surface impurities.

[1] K. F. Mak, C. Lee, J. Hone, J. Shan, and T. F. Heinz, Atomically thin MoS_2: A new direct-gap semiconductor, Phys. Rev. Lett. **105**, 136805 (2010).

[2] P. Tonndorf, R. Schmidt, P. Böttger, X. Zhang, J. Börner, A. Liebig, M. Albrecht, C. Kloc, O. Gordan, D. R. T. Zahn, S. M. de Vasconcellos, and R. Bratschitsch, Photoluminescence emission and Raman response of monolayer MoS_2, $MoSe_2$, and WSe_2, Opt. Express **21**, 4908 (2013).

[3] W. Zhao, Z. Ghorannevis, L. Chu, M. Toh, C. Kloc, P.-H. Tan, and G. Eda, Evolution of electronic structure in atomically thin sheets of WS_2 and WSe_2, ACS Nano **7**, 791 (2013).

[4] L. Schué, L. Sponza, A. Plaud, H. Bensalah, K. Watanabe, T. Taniguchi, F. Ducastelle, A. Loiseau, and J. Barjon, Bright luminescence from indirect and strongly bound excitons in h-BN, Phys. Rev. Lett. **122**, 067401 (2019).

[5] S. Roux, C. Arnold, F. Paleari, L. Sponza, E. Janzen, J. H. Edgar, B. Toury, C. Journet, V. Garnier, P. Steyer, T. Taniguchi, K. Watanabe, F. Ducastelle, A. Loiseau, and J. Barjon, Radiative lifetime of free excitons in hexagonal boron nitride, Phys. Rev. B **104**, L161203 (2021).

[6] L. Schué, B. Berini, A. C. Betz, B. Plaçais, F. Ducastelle, J. Barjon, and A. Loiseau, Dimensionality effects on the luminescence properties of hBN, Nanoscale **8**, 6986 (2016).

[7] C. Elias, P. Valvin, T. Pelini, A. Summerfield, C. Mellor, T. Cheng, L. Eaves, C. Foxon, P. Beton, S. Novikov *et al.*, Direct band-gap crossover in epitaxial monolayer boron nitride, Nat. Commun. **10**, 2639 (2019).

[8] A. Rousseau, L. Ren, A. Durand, P. Valvin, B. Gil, K. Watanabe, T. Taniguchi, B. Urbaszek, X. Marie, C. Robert *et al.*, Monolayer boron nitride: Hyperspectral imaging in the deep ultraviolet, Nano Lett. **21**, 10133 (2021).

[9] K. Watanabe, T. Taniguchi, T. Kuroda, O. Tsuda, and H. Kanda, Time-resolved photoluminescence in band-edge region of hexagonal boron nitride single crystals, Diam. Relat. Mater. **17**, 830 (2008).

[10] K. Watanabe, T. Taniguchi, K. Miya, Y. Sato, K. Nakamura, T. Niiyama, and M. Taniguchi, Hexagonal boron nitride as a new ultraviolet luminescent material and its application – Fluorescence properties of HbN single-crystal powder, Diam. Relat. Mater. **20**, 849 (2011).

[11] X. K. Cao, B. Clubine, J. H. Edgar, J. Y. Lin, and H. X. Jiang, Two-dimensional excitons in three-dimensional hexagonal boron nitride, Appl. Phys. Lett. **103**, 191106 (2013).
[12] G. Cassabois, P. Valvin, and B. Gil, Intervalley scattering in hexagonal boron nitride, Phys. Rev. B **93**, 035207 (2016).
[13] D. D. Nolte, Surface recombination, free-carrier saturation, and dangling bonds in InP and GaAs, Solid-State Electron. **33**, 295 (1990).
[14] J. W. P. Hsu, C. C. Bahr, A. vom Felde, S. W. Downey, G. S. Higashi, and M. J. Cardillo, Si(111)(7 × 7) dangling bond contribution to surface recombination, J. Vac. Sci. Technol. A **10**, 985 (1992).
[15] D. Fitzgerald and A. Grove, Surface recombination in semiconductors, Surf. Sci. **9**, 347 (1968).
[16] L. Jastrzebski, J. Lagowski, and H. C. Gatos, Application of scanning electron microscopy to determination of surface recombination velocity: GaAs, Appl. Phys. Lett. **27**, 537 (1975).
[17] M. Kozák, F. Trojánek, and P. Malý, Large prolongation of free-exciton photoluminescence decay in diamond by two-photon excitation, Opt. Lett. **37**, 2049 (2012).
[18] A. A. High, E. E. Novitskaya, L. V. Butov, M. Hanson, and A. C. Gossard, Control of exciton fluxes in an excitonic integrated circuit, Science **321**, 229 (2008).
[19] L. V. Butov, Excitonic devices, Superlattices Microstruct. **108**, 2 (2017).
[20] L. A. Jauregui and P. Kim, Curved paths of electron-hole pairs, Nat. Mater. **16**, 1169 (2017).
[21] D. Unuchek, A. Ciarrocchi, A. Avsar, K. Watanabe, T. Taniguchi, and A. Kis, Room-temperature electrical control of exciton flux in a Van der Waals heterostructure, Nature (London) **560**, 340 (2018).
[22] F. Cadiz, C. Robert, E. Courtade, M. Manca, L. Martinelli, T. Taniguchi, K. Watanabe, T. Amand, A. C. Rowe, D. Paget, B. Urbaszek, and X. Marie, Exciton diffusion in WSe_2 monolayers embedded in a van der Waals heterostructure, Appl. Phys. Lett. **112**, 152106 (2018).
[23] N. Kumar, Q. Cui, F. Ceballos, D. He, Y. Wang, and H. Zhao, Exciton diffusion in monolayer and bulk $MoSe_2$, Nanoscale **6**, 4915 (2014).
[24] S. Z. Uddin, H. Kim, M. Lorenzon, M. Yeh, D.-H. Lien, E. S. Barnard, H. Htoon, A. Weber-Bargioni, and A. Javey, Neutral exciton diffusion in monolayer MoS_2, ACS Nano **14**, 13433 (2020).
[25] W. Heller, A. Filoramo, P. Roussignol, and U. Bockelmann, Direct measurement of exciton diffusion in quantum wells, Solid-State Electron. **40**, 725 (1996).
[26] C. M. Lawson, R. C. Powell, and W. K. Zwicker, Transient grating investigation of exciton diffusion and fluorescence quenching in Nd_xTa_{1-x} PO crystals, Phys. Rev. B **26**, 4836 (1982).
[27] H. A. Zarem, P. C. Sercel, J. A. Lebens, L. E. Eng, A. Yariv, and K. J. Vahala, Direct determination of the ambipolar diffusion length in GaAs/AlGaAs heterostructures by cathodoluminescence, Appl. Phys. Lett. **55**, 1647 (1989).
[28] N. Ino and N. Yamamoto, Low temperature diffusion length of excitons in gallium nitride measured by cathodoluminescence technique, Appl. Phys. Lett. **93**, 232103 (2008).
[29] M. Hocker, P. Maier, L. Jerg, I. Tischer, G. Neusser, C. Kranz, M. Pristovsek, C. J. Humphreys, R. A. R. Leute, D. Heinz, O. Rettig, F. Scholz, and K. Thonke, Determination of axial and lateral exciton diffusion length in GaN by electron energy dependent cathodoluminescence, J. Appl. Phys. **120**, 085703 (2016).
[30] V. M. Kenkre, Determination of the exciton diffusion constant from variation of quantum yield with penetration length, Chem. Phys. Lett. **82**, 301 (1981).
[31] J. Barjon, F. Jomard, A. Tallaire, J. Achard, and F. Silva, Determination of exciton diffusion lengths in isotopically engineered diamond junctions, Appl. Phys. Lett. **100**, 122107 (2012).
[32] G. Nogues, T. Auzelle, M. D. Hertog, B. Gayral, and B. Daudin, Cathodoluminescence of stacking fault bound excitons for local probing of the exciton diffusion length in single GaN nanowires, Appl. Phys. Lett. **104**, 102102 (2014).
[33] W. Van Roosbroeck, Injected current carrier transport in a semi-infinite semiconductor and the determination of lifetimes and surface recombination velocities, J. Appl. Phys. **26**, 380 (1955).
[34] C. A. Klein, Bandgap dependence and related features of radiation ionization energies in semiconductors, J. Appl. Phys. **39**, 2029 (1968).
[35] B. G. Yacobi and D. B. Holt, *Cathodoluminescence Microscopy of Inorganic Solids* (Springer Science & Business Media, New York, 2013).
[36] K. Kanaya and S. Okayama, Penetration and energy-loss theory of electrons in solid targets, J. Phys. D **5**, 43 (1972).
[37] B. Sieber, Cathodoluminescence—Principes physiques et systèmes de détection, Tech. Ing. Anal. Surf. Materiaux, P3792v1 (10 June 2012).
[38] D. Drouin, A. R. Couture, D. Joly, X. Tastet, V. Aimez, and R. Gauvin, CASINO V2.42–A fast and easy-to-use modeling tool for scanning electron microscopy and microanalysis users, Scanning **29**, 92 (2007).
[39] D. B. Wittry and D. F. Kyser, Measurement of diffusion lengths in direct-gap semiconductors by electron-beam excitation, J. Appl. Phys. **38**, 375 (1967).
[40] S. Liu, R. He, L. Xue, J. Li, B. Liu, and J. H. Edgar, Single crystal growth of millimeter-sized monoisotopic hexagonal boron nitride, Chem. Mater. **30**, 6222 (2018).
[41] J. Li, C. Elias, G. Ye, D. Evans, S. Liu, R. He, G. Cassabois, B. Gil, P. Valvin, B. Liu *et al.*, Single crystal growth of monoisotopic hexagonal boron nitride from a Fe–Cr flux, J. Mater. Chem. C **8**, 9931 (2020).
[42] Y. Kubota, K. Watanabe, O. Tsuda, and T. Taniguchi, Deep ultraviolet light-emitting hexagonal boron nitride synthesized at atmospheric pressure, Science **317**, 932 (2007).
[43] K. Watanabe, T. Taniguchi, and H. Kanda, Direct-bandgap properties and evidence for ultraviolet lasing of hexagonal boron nitride single crystal, Nat. Mater. **3**, 404 (2004).
[44] T. Taniguchi and K. Watanabe, Synthesis of high-purity boron nitride single crystals under high pressure by using Ba-BN solvent, J. Cryst. Growth **303**, 525 (2007).
[45] Y. Li, V. Garnier, C. Journet, J. Barjon, A. Loiseau, I. Stenger, A. Plaud, B. Toury, and P. Steyer, Advanced synthesis of highly crystallized hexagonal boron nitride by coupling polymer-derived ceramics and spark plasma sintering processes—Influence of the crystallization promoter and sintering temperature, Nanotechnology **30**, 035604 (2019).
[46] Y. Li, V. Garnier, P. Steyer, C. Journet, and B. Toury, Millimeter-scale hexagonal boron nitride single crystals for nanosheet generation, ACS Appl. Nano Mater. **3**, 1508 (2020).

[47] A. Plaud, L. Schué, K. Watanabe, T. Taniguchi, A. Loiseau, and J. Barjon, Exciton-exciton annihilation in hBN, Appl. Phys. Lett. **114**, 232103 (2019).

[48] F. Paleari, T. Galvani, H. Amara, F. Ducastelle, A. Molina-Sánchez, and L. Wirtz, Excitons in few-layer hexagonal boron nitride: Davydov splitting and surface localization, 2D Mater. **5**, 045017 (2018).

[49] D.-H. Lien, S. Z. Uddin, M. Yeh, M. Amani, H. Kim, J. W. Ager, III, E. Yablonovitch, and A. Javey, Electrical suppression of all nonradiative recombination pathways in monolayer semiconductors, Science **364**, 468 (2019).

[50] M. Amani, P. Taheri, R. Addou, G. H. Ahn, D. Kiriya, D.-H. Lien, J. W. Ager, III, R. M. Wallace, and A. Javey, Recombination kinetics and effects of superacid treatment in sulfur- and selenium-based transition metal dichalcogenides, Nano Lett. **16**, 2786 (2016).

[51] H. Morimoto, Y. Hazama, K. Tanaka, and N. Naka, Ultrahigh exciton diffusion in intrinsic diamond, Phys. Rev. B **92**, 201202(R) (2015).

[52] M. Onodera, K. Watanabe, M. Isayama, M. Arai, S. Masubuchi, R. Moriya, T. Taniguchi, and T. Machida, Carbon-rich domain in hexagonal boron nitride: Carrier mobility degradation and anomalous bending of the Landau fan diagram in adjacent graphene, Nano Lett. **19**, 7282 (2019).

[53] H. Schlangenotto, H. Maeder, and W. Gerlach, Temperature dependence of the radiative recombination coefficient in silicon, Phys. Status Solidi A **21**, 357 (1974).

[54] O. V. Mikhnenko, P. W. M. Blom, and T.-Q. Nguyen, Exciton diffusion in organic semiconductors, Energy Environ. Sci. **8**, 1867 (2015).

[55] L. Schué, I. Stenger, F. Fossard, A. Loiseau, and J. Barjon, Characterization methods dedicated to nanometer-thick hBN layers, 2D Mater. **4**, 015028 (2016).